ELSEVIER

Journal of Molecular Catalysis A: Chemical 167 (2001) 225–233

JOURNAL OF MOLECULAR CATALYSIS A: CHEMICAL

www.elsevier.com/locate/molcata

Ionic surfactant films imaged by atomic force microscopy

G. Ceotto [a], E.F. de Souza [b], O. Teschke [c,*]

[a] *Departamento de Fisica, Universidade Federal de Vicosa, 36571-000 Vicosa, MG, Brazil*
[b] *Instituto de Ciencias Biologicas e Quimica, Pontificia Universidade Catolica de Campinas, 13020-904 Campinas, SP, Brazil*
[c] *Nano-Structure Laboratory, IFGW/UNICAMP, 13081-970 Campinas, SP, Brazil*

Received 6 April 2000

Abstract

Forces acting on atomic force microscope (AFM) tips responsible for image formation are measured during scanning of films of ionic surfactant molecules adsorbed from aqueous solutions onto hydrophilic substrates. Near the critical micelle concentration mica substrate images show aggregate regions at the interface. Force versus distance measured curves show that patches form a thicker structure than the formed at partially covered regions, in agreement with the fact that at patches the adsorbates are perpendicularly oriented to the substrate plane. However, AFM topographic images registered at low scanning speed (5 μm/s) show that these patched regions appear as holes, forming inverted images. In AFM imaging of soft structures, as surfactants or biological material, inverted in contrast with images may be observed when there is a specific tip penetration through each scanned layer. This penetration is adjusted by changing the tip force set point, consequently different topographic profiles are obtained. The precise force set point to obtain the correct contrast in scanned images is obtained by the analysis of the force versus distance curves that show the normal to the scanned plane structure profile. Adsorption patterns as a function of time may be conveniently monitored and the adsorption rate may be determined. © 2001 Published by Elsevier Science B.V.

Keywords: Ionic surfactant; Adsorbed films; AFM imaging; Adsorption dynamics

1. Introduction

Understanding the adsorption mechanism of surfactant molecules at the solid–liquid interface, is an important step toward modeling industrial processes which use surfactants on a large scale, such as detergency, water purification, oil recovery, and ore refinement by flotation [1]. An intermolecular interaction in bulk solution leads to a variety of self-assembled structures like micelles or liquid-crystalline structures which have been well-studied [2]. At an interface, however, the normal self-assembly process is perturbed by competing surfactant–surface and solvent–surface interactions, which can, in principle, lead to novel structures termed ‘hemimicelles’ [3]. Over the last few decades, the adsorption characteristics of a wide variety of surfactant–solvent–substrate systems have been investigated, traditionally by adsorption isotherm [4] and more recently by fluorescence decay [5] and neutron reflection [6].

Imaging hard samples with atomic resolution requires a probe with atomic dimensions. The atomic force microscope (AFM) obtains its topographical information from the short-ranged repulsion resulting from the overlap of electronic shells between tip and sample [7]. However, the presence of long-ranged interactions such as the double layer electrostatic force

* Corresponding author. Fax: +55-19-788-5376.
E-mail address: oteschke@ifi.unicamp.br (O. Teschke).

1381-1169/01/$ – see front matter © 2001 Published by Elsevier Science B.V.
PII: S1381-1169(00)00510-0

[8–12] when scanning soft samples in liquid media leads to a very different imaging scenario. The purpose of this paper is to report on forces acting on the tip when imaging soft samples, as surfactant layers, in liquid media; and determine their effects on the AFM image contrast.

2. Experimental

Adsorption and self-assembly of the cationic surfactant cetyltrimethylammonium bromide (CTAB, $C_{16}H_{33}$–$N^+(CH_3)_3Br^-$, CMC = 0.9 mM) was investigated at the interface between an aqueous solution and a hydrophilic substrate, namely the cleavage plane of mica. Surfactant adsorption was accomplished by introducing an aqueous solution of CTAB into the fluid cell and allowing the tip and freshly cleaved substrate to stand in this solution for 50 min before operation. CTAB (99% purity) was used as supplied, without further purification. CTAB aqueous solutions using Milli-Q Plus quality (resistivity ∼15 MΩ/cm) were introduced into the cell after freshly cleaved mica was mounted on the *xyz* translator of the AFM.

In this study force curves and images were obtained in surfactant solution and water at room temperature (∼25°C) by a commercial AFM (Topometrix TMX2000). A sensor using a four-quadrant detector measures vertical as well as lateral forces. Unmodified silicon nitride (Si_3N_4) tips [13] (Microlever™, type B, Park) was used. A special cell was built in order to perform observations in liquid media [14,15]. The cell was made of Teflon™ and the substrate (freshly cleaved mica) was fixed at its bottom. It was mounted in an *xyz* piezotranslator to position the sample in contact with a stationary tip. The laser beam enters and leaves the cell through a glass plate and thus does not cross the air–liquid interface, which is usually curved. We have obtained best results in these measurements with very soft cantilevers, typically ∼0.02 N/m. The instrument was calibrated and the measured spring constant in air (0.023 nN/nm) was found to agree with that specified by the cantilever manufacturer.

When the mica basal plane is placed in pure water, the mechanism for the formation of the double layer is assumed to be the dissolution of K^+ ions as well as ion exchange of K^+ by H^+ or H_3O^+ ions. When CTAB is added to water K^+ is also substituted by $C_{16}H_{33}(CH_3)_3N^+$ ions. The ζ (zeta) potential at the macroscopic mica surface–water interface, was measured using the plane-interface technique in the presence of 10^{-3} M KCl, and was found to be ∼125 mV within 5–6 pH range [16].

3. Results and discussion

Fig. 1 shows an image taken at a CTAB concentration of about 5×10^{-5} M. For this concentration a light region and a few CTAB patches (dark regions) are observed, as previously reported [17,18]. The standard AFM contrast in images show high structures as light regions and low structures as dark, consequently a high structure with a few holes covers the observed area. An apparent height difference between the two layers (dark and light regions) of 0.5 nm was measured for a scanning speed of 15 μm/s. In order to determine the film thickness of each layer, force versus distance curves at the patches and at light regions were measured. Initially, a control experiment was performed by measuring force versus distances curves for mica immersed in water. The result is shown in Fig. 2a by curve (□). Observe that there is no repulsive component at distances a few nanometers away from the substrate, indicating that there is no adsorbed structure at the interface. In force versus distance curves [19], the vertical axis represents the force acting between tip and sample surface. Its value is obtained by multiplying the deflection of the cantilever with its spring constant. The horizontal axis (x) represents the distance the sample is moved perpendicular to the surface by the *xyz* translator. In this curve, repulsion and attraction acts between tip and sample before contact. Hence, when the sample approaches the tip, the cantilever bends upwards. At a certain point the tip is attracted to the surface. Finally, moving the sample still further causes a deflection of the cantilever by the same amount the sample is moved. A typical approaching force curve collected on a mica surface in CTAB solutions is a plot of the change in cantilever deflection (ΔY) versus sample displacement (ΔX). On a hard and nondeformable surface, ΔY is proportional to ΔX while the tip and the sample are in contact. Rather than using sample position (X), it is more useful to use an absolute distance (D), i.e. the separation between the tip and the sample surface. The correction

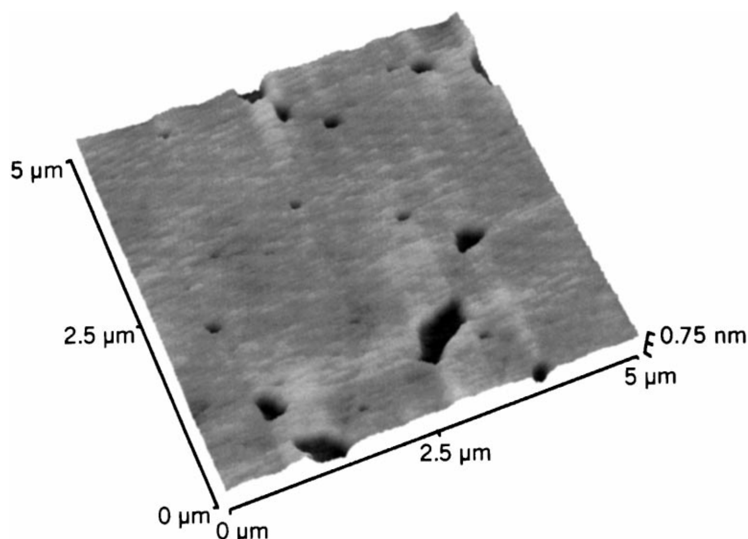

Fig. 1. AFM image of a CTAB adsorbed layer on mica in a 10^{-5} M CTAB solution. Lighter regions indicate higher structures.

to produce a force versus distance curve uses the relationship $D = \Delta X - \Delta Y$ [20]. Fig. 2a shows the force versus absolute distances for the light area (curve (◇)), the patch region (dark region, curve (○)) and water (curve (□)). The inset corresponds to the same curve shown in the main figure in an extended scale.

The analysis of Fig. 2a shows that, at distances far away from the surfactant layer, there is a force field that decays exponentially with distance with a Debye's length (L_D) ~27 nm, similarly to the one obtained for bare mica in water ($L_D \approx 60$ nm), curve (□), in agreement with the value measured by Kékicheff et al. [21]. The force intensity is decreased, approximately, by a factor of 3 when compared with the value measured in water. This indicates the presence of an electric field, generated by surface electric charges (mica), partially neutralized by surfactant adsorbed layer charges with the head groups in contact with the mica surface and exposed to the aqueous phase.

The strong repulsive forces at regions close to the substrate interface (<5 nm, Fig. 2b), in both curves ((○), patches and (◇), light region forming the background structure), are associated with the adsorbed surfactant layer [17,22]. According to Tanford [23], the calculated fully extended molecular length of the chain is $L_{max} \approx (0.15 + 0.1265n)$ nm $= 2.17$ nm, where $n = 16$ is the number of saturated hydrocarbon chain. The published results of Campanelli and Scaramuzza [24] indicate that the fully extended molecular length is ~2.16 nm. In our experiments we observe, for light regions (curve (◇), Fig. 2b), a strong repulsive force beginning at about 2.5 nm from the surface with a rapid change in force with a small change in tip/surface separation at $\sim 2.3 \pm 0.1$ nm from the mica surface.

A different surfactant structure is formed at the dark regions (Fig. 2b, curve (○)) as observed by the large repulsive deviation from exponential component starting about 4.2 nm from contact and reaching a steep wall at ~4.0 nm [17,22,25]. A rapid change in force with almost no change in tip/substrate separation (at about 4.0 nm) followed by a second attractive regime (3.2 nm) is observed when the tip approaches the interface. This indicates that the layer compression is followed by an attraction of the tip by the remaining material between the tip and substrate.

The distance measured from the contact point ($D = 0$) to the region of a sharp increase in the force value gives the surfactant layer thickness. The measured thickness of patches and of the light background region are ~4.0 and 2.4 nm, respectively; dark areas are then thicker than light regions, and the film thickness difference measured from these curves is ~1.6 nm. At sufficiently large applied force, the surfactant layer is

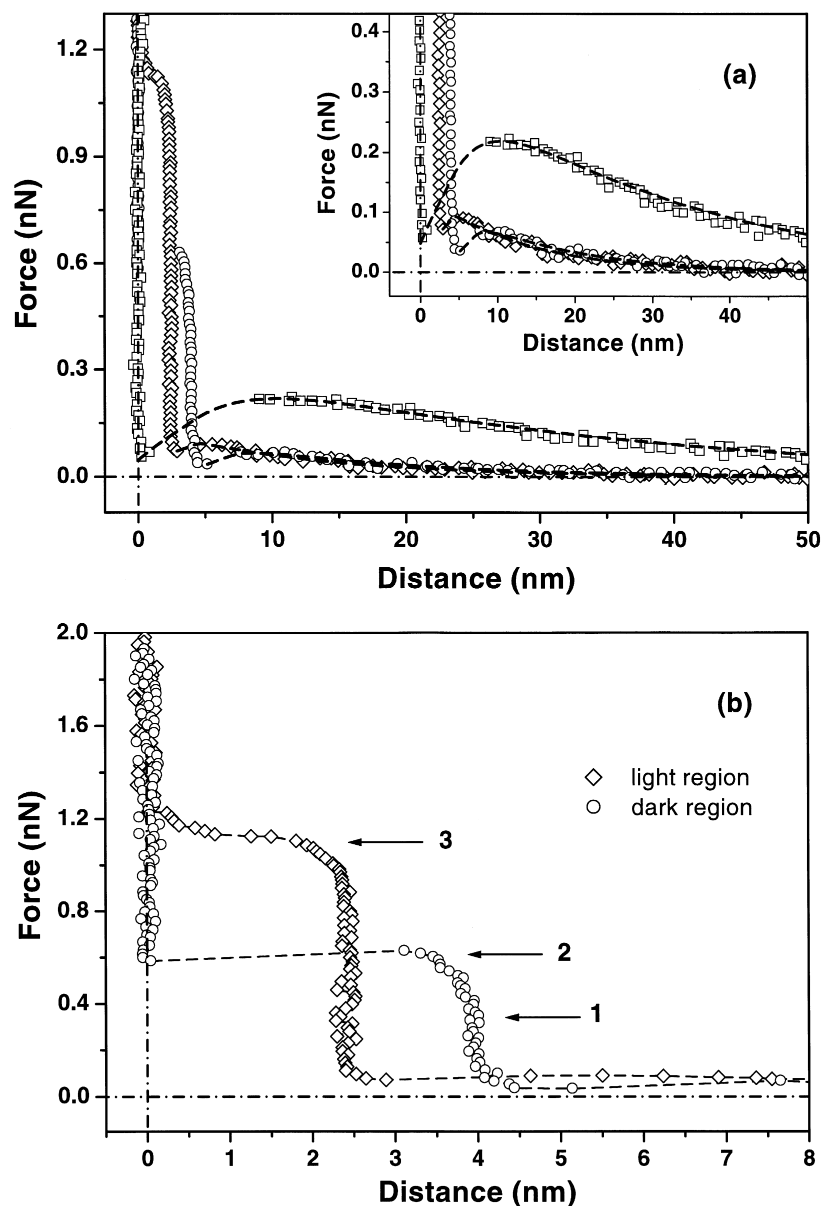

Fig. 2. (a) Force vs. absolute distance curves for water (□), dark region (patches (○)) and light region (◇). Dashed lines are drawn to guide the eyes. Inset, same curve showing the details of the force acting on the tip when immersed in the diffuse double layer. (b) The same force vs. distance curves displayed in a region close (<8 nm) to the mica surface: dark region (curve (○)) and light region (curve (◇)).

squeezed from the space between the tip and the surface. This value is defined as the film rupture force and it is equal to 1.25 nN for the light region and 0.5 nN for the dark region. Previous results identify this rupture force with steric limitations imposed by the immobilization of CTAB and by the location of the CTAB binding site at the mica surface [26].

The topographic image in Fig. 1 shows that the dark region form shorter structures than the background, but the force versus distance curves show that the mea-

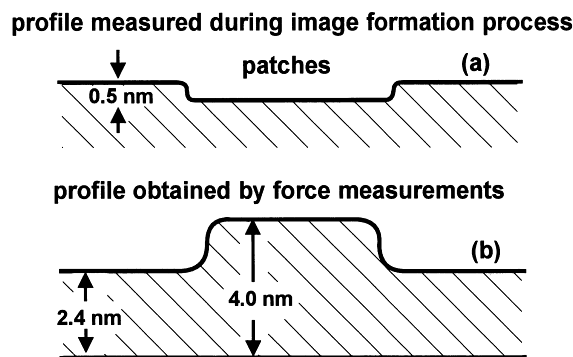

Fig. 3. Schematic diagram of the different stages present during sample scanning and the force vs. distance measurements depict by the relative height of the adsorbed structures.

sured thickness of the dark region is 4.0 nm, and of the light region, 2.4 nm. The height variation of the different adsorbed structures measured during the scanning process and in the force versus distance curves acquisition stages are shown in Fig. 3. In order to explain the inverted in contrast image, conforming to the AFM practice that high structures are light and low structures are dark, the effect of the scanning speed on the image contrast was investigated. An extra force associated with the scanning movement acts on the tip. A simple analogy for the observed phenomena is water skiing. In water skiing, the ski has to move faster than the water surface can rearrange. Consequently, the variable dynamic normal forces associated with the tip skiing at various scan speeds prevent the tip from penetrating through the layer. When comparing the measured height difference in Fig. 1, for dark and light regions, it is possible to determine, for each scanning speed, the value of the vertical force associated with the skiing of the tip. Since the measured height difference between the dark and the light region images in Fig. 1 is 0.5 nm, it is possible to determine the force component resulting from the tip skiing by determining the amplitude, in the force versus distance curves, that correspond to a height difference of 0.5 nm. The tip effective force is indicated by 2 in Fig. 2b, which corresponds to normal component of the skiing force of 2.0 nN (force set point 2.56 nN).

The effect of the tips scanning speed on the image is observed in Fig. 4a–c, which display the pattern obtained for a force set point of 2.56 nN and the following scanning speeds: (a) 15; (b) 50 and (c) 100 μm/s. From 15 to 50 μm/s curves show identical images. For scanning speed >50 μm/s, the shape of the patches is drastically modified at each scanning. Inverted in contrast images were obtained for all scanning speeds, consequently, for the range of tested scanning velocities, no effect on the image contrast was observed.

An experiment was then performed, where an area was scanned for a constant scanning speed but with different tip applied forces. The result is given in Fig. 5a–c shows the image obtained by scanning a mica CTAB covered region with a contact force of 2.56 nN; Fig. 5b shows the same scanned region divided in three sub-sets, each scanned with a different applied force: 2.56 (top), 0.12 (middle) and 3.66 nN (bottom). Finally, Fig. 5c was registered immediately after the scanning shown in Fig. 5b. This image was also obtained with a contact force of 2.56 nN. The spatial distribution of the adsorbed surfactant layer on mica is shown in all images; the dark areas correspond to the patch regions and they are distributed in a background of a light region. Inverted in contrast images are obtained for all measured applied forces. The effect of a variable applied force is quantified by measuring the height difference between patches and the light region for the three applied forces: ~0.5, 0.3 and 0.7 nN, respectively. The penetration of the tip through the light region and patches and consequently the AFM image contrast depends, then, on the applied force set point value.

The image shown in the bottom part of Fig. 5b presents a large number of small dark regions (patches) which were not present in the first scanned image. Since this image was obtained for the largest tip penetration through the surfactant layer it would be reasonable to assume that the removal of molecules from the light region will result in the formation of new small patches of surfactant molecules. Finally, in Fig. 5c we observe that after successive scans small patches tend to regroup, forming regions of larger patches.

Dark areas were then observed. The determining role played by the applied force set point in the image contrast is established when we change the applied force from 0.012 (Fig. 6a) to 2.56 nN (Fig. 6b); a change in contrast occurred when the tip force was increased.

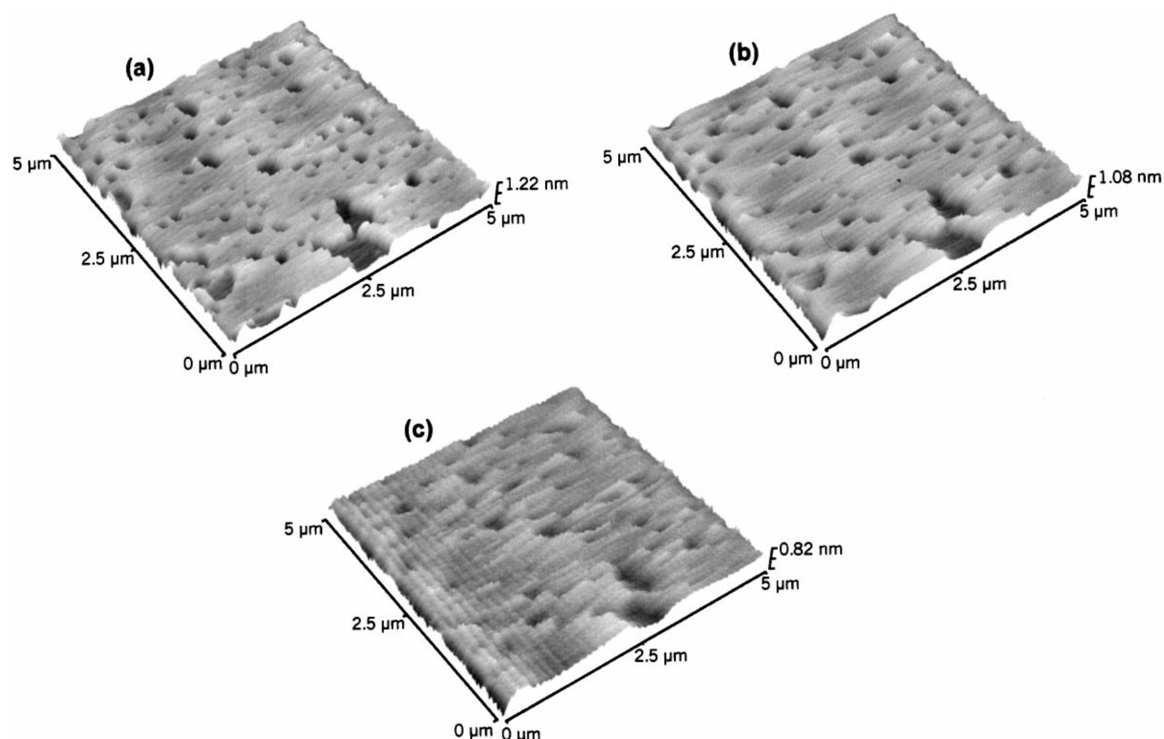

Fig. 4. AFM images of the solution/surfactant/mica interface for 2.56 nN applied force showing the tip scanning speed effect: (a) 15; (b) 50 and (c) 100 μm/s.

Considerable forces between the tip and sample are a requirement for AFM imaging. For hard samples, like mineral surfaces, these forces do not, generally, lead to any sample penetration. However, for organic films the minimum forces, which are barely enough to allow stable imaging, result in tip penetration in each structure shown in Fig. 1 by the dark and light regions. In order to obtain the conventional AFM contrast in the scanned samples, an analysis of the force versus distance curves is a requirement as follows: let us observe Fig. 2b and consider the following simple scenario where we have an almost null vertical component due to the tip skiing. At the light region (curve (◇)), by setting the contact force at 0.6 nN the tip is contacting the top of the surfactant layer. When the tip reaches the dark region the repulsive force is smaller than at the light region. Consequently, the tip gets closer to the substrate. A scanning profile that shows a smaller tip to substrate separation at the patch region than at the substrate is then registered, forming an inverted in contrast image. If the applied tip force varies from ~0.6 to 1.2 nN the same contrast image is obtained.

The total force on a tip when scanning is the sum of the vertical force component associated with the tip skiing and the applied force. The true image profile of the surfactant structure would be obtained if the sum of forces on the tip (the sum of the applied force set value and the normal component force associated with the tip skiing) corresponds to the value indicated by 1 in Fig. 2b up to a total force of 0.5 nN. From these curves the patch height measured value is ~4.0 nm and the light region height is ~2.4 nm, as indicated by curves (◇) and (○).

The data obtained by force versus distance curves is then a requirement, in order to determine the tip applied force set value for registering the AFM standard contrast in imaging surfaces and measuring the true layer thicknesses. Large values of the sum of forces on the tip will result in the removal of the adsorbed layer, as indicated by 3 in Fig. 2b, medium

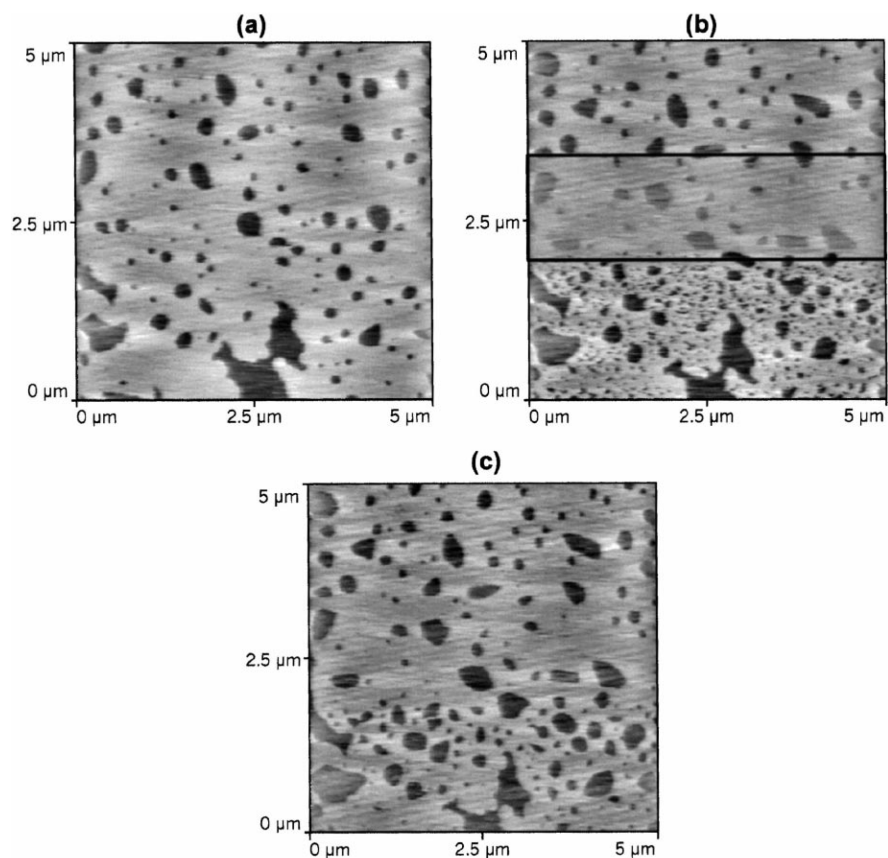

Fig. 5. AFM images of the solution/surfactant/mica interface showing the tip force set point effect: (a) applied force of 2.56 nN, scanning speed 15 µm/s; (b) the region was scanned for different tip applied forces top 2.56 nN, middle 0.12 nN and bottom 3.66 nN; (c) image obtained after the scanned image shown in (b) for a tip applied force of 2.56 nN.

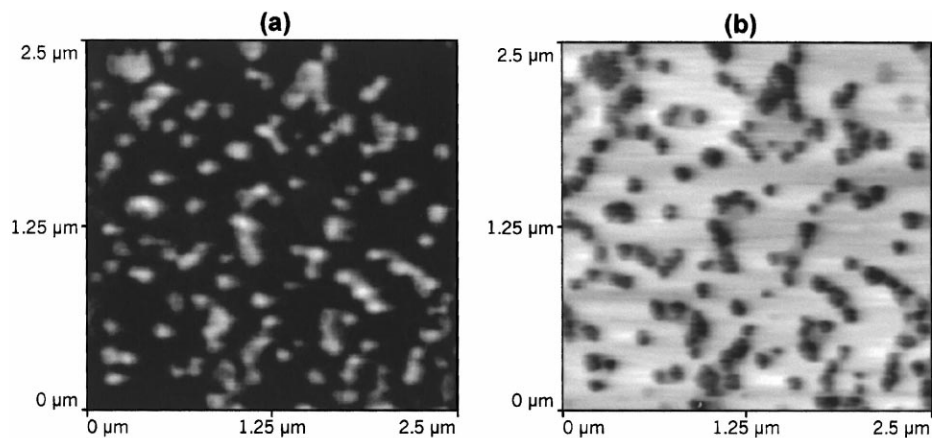

Fig. 6. AFM images of the solution/surfactant/mica interface scanned at different applied tip forces showing a change in image contrast: (a) 0.012 and (b) 2.56 nN.

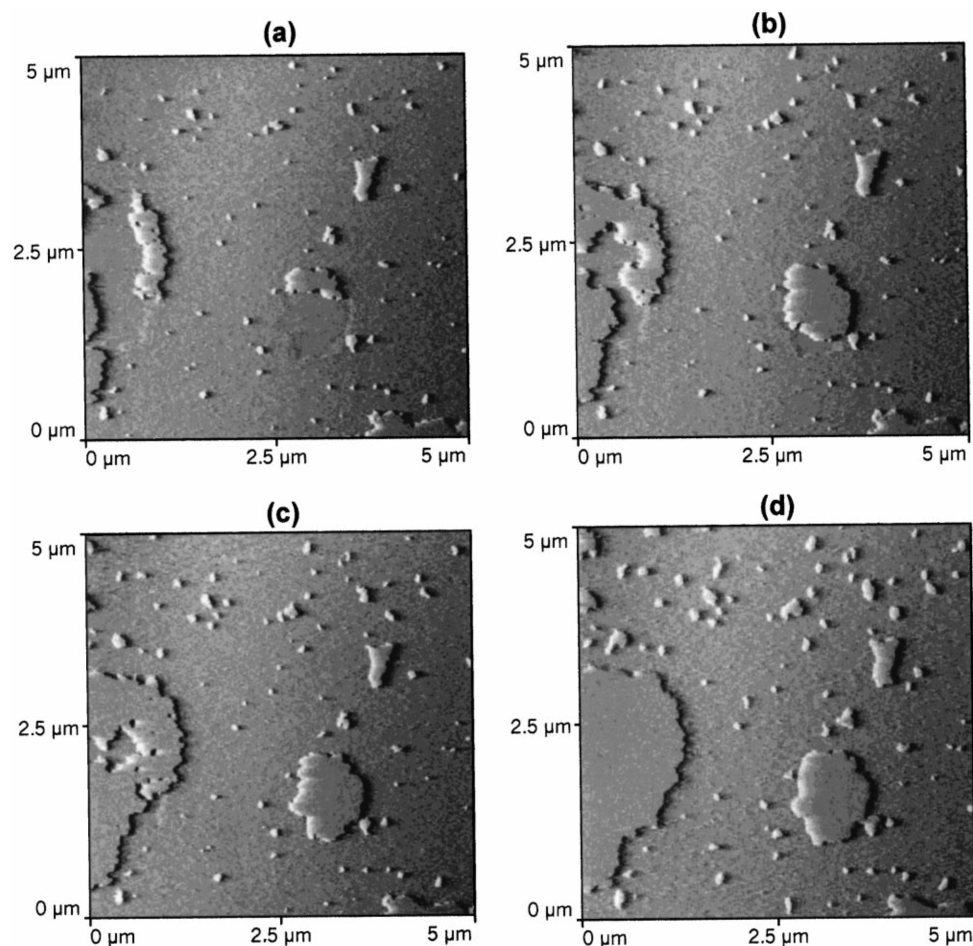

Fig. 7. Adsorbed surfactant patterns observed at mica surfaces immersed in 1×10^{-5} M CTAB aqueous solution. Different aggregate sizes adsorbed at the interface for various immersion times: (a) 25; (b) 45; (c) 60 and (d) 105 min. Differentiated growth coefficient may be observed for various sized patches.

forces result in inverted in contrast images as indicated by 2 in Fig. 2b, and the conventional image contrast is obtained for small forces, as indicated by 1 in Fig. 2b.

The measured width of the surfactant layers indicate that we have monolayers and bilayers adsorbed at the mica interface. Force versus distance measurements shown in Fig. 2 show that the patches have an ∼3.2 nm width which corresponds the CTAB bilayer length. This thickness measured value is in good agreement with that determined by Pashley et al. (3.3 nm) [27], Kékicheff et al. (3.2 nm) [21] and Fragneto et al. (3.2 nm) [28]. The adsorbed structure forming the background has ∼2.2 nm width corresponding to the length of a CTAB molecule (monolayer). On the force curves, the effect of surfactant molecules adsorbed on the tip at the interfacial region is much smaller than the ones adsorbed at the mica interface, since the tip is almost neutral and the mica surface is negatively charged which will attract the positively charged surfactant molecule.

After adjusting the tip force set point during sample scanning in order to obtain the true image contrast it is possible to monitor the time dependence size of the surfactant aggregates adsorbed at the mica surface.

Fig. 7 shows (1×10^{-5} M CTAB) different aggregate sizes adsorbed at the interface for various immersion times: (a) 25; (b) 45; (c) 60 and (d) 105 min. The intriguing aspects of the interfacial growth is that different sized patches adsorbed next to each other, show differentiated growth coefficients. The distinct local growth coefficient is attributed to either impurities effects in interfacial kinetics [29–32] or two-dimensional (2D) nucleation and spreading of 2D islands.

Adsorbed patches size distribution measurements via reflectometry are diffraction-limited, i.e. patches are only observed for sizes larger than the incident visible radiation wavelength ($\lambda \approx 500$ nm). Here, patch sizes as small as 50 nm had their time dependent growth measured.

4. Conclusions

Images of soft layers have been previously reported [18,22,26,33,34]. Here, the effect of the applied force on the AFM image contrast was investigated. Patches formed by solvent–surfactant–substrate systems at mica surfaces in CTAB solutions were imaged and also characterized by force versus distance measurements. Fluid membranes can be imaged stable with a variable apparent height difference between various layers depending on the tip applied contact force. By adjusting the applied force and the scanning velocity the conventional contrast may be obtained in imaging soft adsorbed layers. The tip force set point value, needed to obtain the true profile of the structures, is determined from the force versus distance curves, which show the force component normal to the scanned plane. High applied tip forces when scanning soft material will result in the removed adsorbed layer, medium forces result in inverted contrast images and the true image contrast is only obtained for small applied forces.

Acknowledgements

The authors thank J.R. Castro and L.O. Bonugli for technical assistance. This study was supported by the CNPq grant 523.268/95-5 and FAEP/UNICAMP grant 45/00.

References

[1] A.W. Adamson, Physical Chemistry of Surfaces, 5th Edition, Wiley, New York, 1990 (Chapter XIII).
[2] J.N. Israelachvili, Intermolecular and Surface Forces, 2nd Edition, Academic Press, London, 1992.
[3] A.M. Gaudin, D.W. Fuerstenau, Trans. AIME 202 (1955) 958.
[4] J.J. Kipling, Adsorption from Solution of Non-Electrolytes, Academic Press, London, 1965.
[5] P. Chandar, P. Somasundaran, N.J. Turro, J. Colloid Interface Sci. 31 (1987) 117.
[6] D.C. McDermott, J. McCarney, R.K. Thomas, A.R. Rennie, J. Colloid Interface Sci. 162 (1994) 304.
[7] F.V. Giesseibl, Rev. Phys. B 45 (1992) 13815.
[8] O. Teschke, E.F. de Souza, Appl. Phys. Lett. 74 (1999) 1755.
[9] O. Teschke, E.F. de Souza, Rev. Sci. Instrum. 69 (1998) 3588.
[10] I.Y. Sokolov, G.S. Henderson, F.J. Wicks, G.A. Ozin, Appl. Phys. Lett. 70 (1997) 844.
[11] S. Manne, J.P. Cleveland, H.E. Gaub, G.D. Stucky, P.K. Hansma, Langmuir 10 (1994) 4409.
[12] W.A. Ducker, T.J. Senden, Langmuir 8 (1992) 1831.
[13] Thermomicroscopes, 1171, Borregas Avenue, Sunnyvale, CA 94089, USA.
[14] O. Teschke, R.A. Douglas, T.A. Prolla, Appl. Phys. Lett. 70 (1997) 1977.
[15] R.M. Sassaki, R.A. Douglas, M.U. Kleinke, O. Teschke, J. Vac. Sci. Technol. B 14 (1996) 2432.
[16] R.J. Hunter, Foundations of Colloid Science, Oxford University Press, New York, 1997.
[17] D.J. Neivandt, M.L. Gee, M.L. Hair, C.P. Tripp, J. Phys. Chem. B 102 (1988) 5107.
[18] B.G. Sharma, S. Basa, M.M. Sharma, Langmuir 12 (1996) 6506.
[19] W.A. Ducker, T.J. Senden, R.A. Pashley, Langmuir 8 (1992) 1831.
[20] H.J. Butt, M. Jaschke, W.A. Ducker, Bioelectrochem. Bioenerg. 38 (1995) 191.
[21] P. Kékicheff, H. Christenson, B.W. Ninham, Colloids Surf. 40 (1989) 31.
[22] M.W. Rutland, J.L. Parker, Langmuir 10 (1994) 1110.
[23] C. Tanford, The Hidrophobic Effect, Wiley, New York, 1973, 1980.
[24] A.R. Campanelli, L. Scaramuzza, Acta Cryst. C42 (1986) 1380.
[25] S. Manne, J.P. Cleveland, H.E. Gaub, G.D. Stucky, P.K. Hansma, Langmuir 10 (1994) 4409.
[26] V. Yaminsky, C. Jones, F. Yaminsky, B.W. Ninham, Langmuir 12 (1996) 3531.
[27] R.M. Pashley, P.M. McGuiggan, R.G. Horn, B.W. Ninham, J. Colloid Interface Sci. 126 (1988) 569.
[28] G. Fragneto, R.K. Thomas, A.R. Rennie, J. Penfold, Langmuir 12 (1996) 6036.
[29] S.R. Coriell, R.F. Sekerka, J. Cryst. Growth 61 (1983) 499.
[30] D. Kandel, J.D. Weeks, Phys. Ver. Lett. 69 (1992) 3758.
[31] D. Kandel, J.D. Weeks, Physica D 66 (1993) 78.
[32] D. Kandel, J.D. Weeks, Phys. Rev. B 49 (1994) 5554.
[33] J. Radler, M. Radmacher, H.E. Gaub, Langmuir 10 (1994) 3111.
[34] G.S. Blackman, C.M. Mate, M.R. Philpott, Phys. Rev. Lett. 65 (1990) 2270.